Coherence analysis of noise-like pulses generated by an erbium-doped fiber mode-locked laser*

ZHANG Ziyi, WANG Chuncan, LI Jing, and WANG Peng**

Key Laboratory of All Optical Network and Advanced Telecommunication Network, Ministry of Education, Institute of Lightwave Technology, Beijing Jiaotong University, Beijing 100044, China

(Received 15 July 2023; Revised 9 October 2023)

The noise-like pulses (NLPs) with tunable fraction of the pedestal height in the whole intensity autocorrelation (AC) trace are numerically demonstrated in the designed erbium-doped fiber (EDF) mode-locked laser, which contains the saturable absorber (SA) with nonlinear polarization rotation (NPR), sinusoidal-shaped or Gaussian-shaped filter, two segments of EDFs, and two pieces of single-mode fibers (SMFs) with normal dispersion and anomalous dispersion, respectively. The pedestal ratio of the intensity AC trace can be tuned by changing the gain saturation energies of EDFs. The results show that when the net cavity dispersion is 1.06 ps^2, the tuning range of the pedestal ratio for the NLPs can reach its maximum values, which are 0.51—0.89 and 0.58—0.88 for the sinusoidal-shaped and Gaussian-shaped filters, respectively. In addition, an appropriate choice of filter bandwidth is also conducive to obtain a wide range of the tuning pedestal ratio for the intensity AC trace.

Document code: A **Article ID:** 1673-1905(2024)04-0205-6
DOI https://doi.org/10.1007/s11801-024-3133-2

Passive mode-locked fiber lasers are widely used in material processing, optical sensing, spectroscopy and biomedicine because of their compactness, high efficiency and high beam quality. Generally, the pulse operating state of passive mode-locked fiber lasers can be divided into two categories[1], coherent and incoherent ones. The former case includes conventional solitons[2], dispersion-managed solitons[3], self-similarity[4], dissipative solitons[5] and dissipative solitons resonance[6]. The latter case is mainly noise-like pulses (NLPs)[7]. Two pulse states have their own advantages, among which the NLP fiber laser shows the characteristics of broadband[8,9], high energy[10], tunable abilities of harmonic order[11] and center wavelength[12,13] and low coherence[14]. Especially its low coherence makes it useful in the field of grating sensing array demodulation[15], optical coherence tomography technology[16], optical data storage and recovery[17] and so on.

NLP is composed of a series of sub-pulses with different amplitudes and phases, similar to a wave packet. The special intensity autocorrelation (AC) trace is one of the unique features of NLP. Since the AC trace consists of a very wide pedestal and narrow peaks, NLP is also called double-scale pulse[18]. The width of the pedestal in the intensity AC trace is equal to the temporal width of the wave packet, and the average pulse width of an ultrashort pulse in the wave packet is related to the peak width. The closer the pedestal ratio is to 0.5, the more random the sub-pulses are. As a result, the increase of the pedestal ratio is helpful in improving the coherence of the sub-pulses[19].

It had been demonstrated that NLP can be obtained in both cases with normal and anomalous net-cavity dispersion. For the former case, XU et al[20] systematically investigated the influences of filtering effects with Gaussian-shaped, super Gaussian-shaped and sinusoidal-shaped filters on the evolution of NLPs in Yb-doped fiber mode-locked lasers, where the net-cavity dispersion in the fiber lasers is 1.03 ps^2. The results show that the ratio of pedestal height in the NLP AC trace can reach its maximum value of about 0.82 by using the sinusoidal filter. Based on semiconductor saturable mirror (SESAM), LI et al[12] reported that the pedestal ratios of the intensity AC trace of NLP is about 0.62 which is realized in an erbium-doped fiber (EDF) laser with net dispersion of 0.095 ps^2. LI et al[21] reported the controllable generation of different pulse modes in fiber lasers including the NLP, by using the pulse power editing (PPE) technique. When the net cavity dispersion is 0.041 7 ps^2, the pedestal ratio can reach up to 0.9. For the thulium-doped fiber ring laser cavity with anomalous net-cavity dispersion in the range of −1.425—14.877 ps^2, LIU et al[22] obtained NLP with the pedestal ratio of about 0.65. TANG et al[23] demonstrated experimentally that an EDF mode locked ring laser with a net-cavity dispersion of −0.04 ps^2 can obtain NLP with pedestal

* This work has been supported by the National Natural Science Foundation of China (No.61575018).
** E-mail: chcwang@bjtu.edu.cn

ratio of about 0.45. LEI et al[24] proposed a mode-locked fiber laser based on nonlinear polarization rotation, and obtained pedestal ratios of about 0.45 when the net-cavity dispersion is −0.090 87 ps^2. It can be seen the pedestal ratios in the intensity AC trace of NLPs obtained in the normal-dispersion laser cavities are relatively higher than those in the anomalous dispersion laser cavities.

At present, there have been many researches on generation methods[25-27] and principles of NLP[23,28]. However, to the best of my knowledge, there are few reports about realizing the tunable pedestal ratio in the intensity AC trace of NLPs. Since the pedestal ratio of the intensity AC trace of NLPs is dependent on the coherence of the sub-pulses, it is very interesting to realize the NLP mode-locked fiber laser with tunable pedestal ratios for expanding its application scenarios.

Compared with a series of previous studies, it is found that the value of the net-cavity dispersion has a great influence on the pedestal ratio of the NLP intensity AC trace. However, for a fixed laser configuration, adjusting the net-cavity dispersion means changing the length of the fiber, which is a very tedious work for the structural adjustment of the laser in the experiment. Therefore, we propose to adjust the pedestal ratio of the NLP intensity AC trace by adjusting the gain saturation energy of the active fiber.

Fig.1 shows the simulation model of the EDF mode-locked laser based on a ring cavity configuration. The EDF mode-locked laser consists of two EDF segments, a piece of single-mode fiber (SMF), a piece of dispersion-compensated fiber (DCF), a polarization dependent isolator (PD-ISO), polarization controllers (PC), an optical coupler (OC) with 50% laser output and a filter. The fiber parameters used in the simulation are shown in Tab.1[29,30].

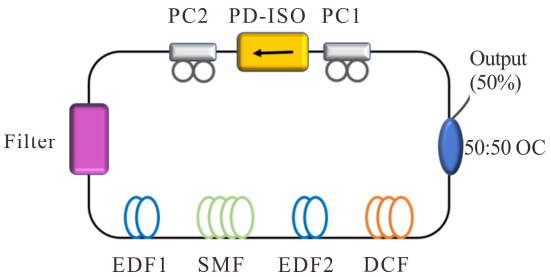

SMF: single-mode fiber; EDF: erbium-doped fiber; DCF: dispersion compensation fiber; OC: optical coupler; PC: polarization controller; PD-ISO: polarization dependent isolator

Fig.1 Schematic of the EDF mode-locked ring cavity laser based on nonlinear polarization rotation

The spectral filter can be used to suppress the amplified spontaneous emission in mode-locked fiber lasers for the purpose of obtaining the stable operation. On the other hand, the NLPs with tunable central wavelength can be obtained by tuning the central wavelength of the filter[12,31].

Tab.1 Fiber parameters used in the simulation

Fiber	L (m)	β_2 (ps^2/m)	β_3 (ps^3/m)	γ (W^{-1}m^{-1})
EDF1	0.5	1.5×10^{-2}	5×10^{-5}	3.2×10^{-3}
EDF2	0.5	1.5×10^{-2}	5×10^{-5}	3.2×10^{-3}
SMF	1 (varied)	-2.3×10^{-2}	8.6×10^{-5}	1.0×10^{-3}
DCF	6 (varied)	1.78×10^{-1}	5.2×10^{-4}	5.7×10^{-3}

In addition, the simulation results shows that when the coupling ratios of the OC are 20: 80, 30: 70 and 40: 60, the laser cannot operate in the stable NLP state, as shown in Fig.2(a)—(c). Fig.2(d) exhibits a stable NLP output with the coupling ratio of 50: 50. When the ratio of the optical power returned to the cavity increases beyond 60%, the temporal durations of output NLPs increase with the coupling ratio, as shown in Fig.2(e)—(h). Meanwhile, the decreased loss in the cavity can also lead to the output NLPs with broadened spectra. As a result, the simulations require more wider calculation windows both in the time and frequency domains, which will dramatically increase the calculation amount. Therefore, the coupling ratio is set to 50: 50 after taking comprehensive factors into account.

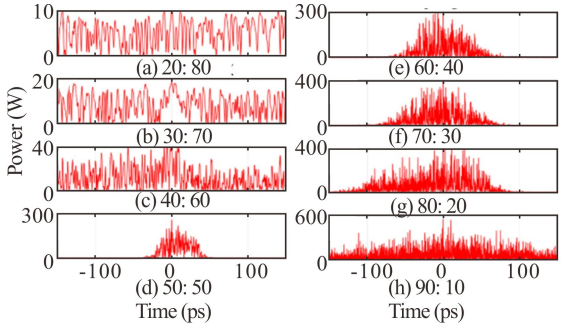

Fig.2 Output pulse temporal envelopes under different coupling ratios when the net-cavity dispersion is 1.06 ps^2, E_{sat1}=0.6 nJ and E_{sat2}=0.8 nJ (The coupling ratio here is defined as the ratio of the optical power returned to the cavity to that at the output port)

In the simulation process, quantum noise (QN) is taken as the initial condition of modeling the mode-locked EDF laser, and can be expressed as[32]

$$\delta_{QN} = (h\omega_m / \Delta\Omega)^{1/2} \exp(i2\pi\Phi_m), \quad (1)$$

where h is Planck constant, and Φ_m is the random value in the range of 0—1.

The pulse evolution in the EDF mode-locked laser can be described by the generalized nonlinear Schrodinger equation (GNLSE)[33,34]

$$\frac{\partial A}{\partial Z} - \frac{g}{2}A + \frac{i\beta_2}{2}\frac{\partial^2 A}{\partial T^2} - \frac{\beta_3}{6}\frac{\partial^3 A}{\partial T^3} + \frac{\alpha}{2}A =$$
$$i\gamma\left(1 + \frac{i}{\omega_0}\frac{\partial}{\partial T}\right)A(z,T)\int_0^\infty R(t')\,|A(z,T-t')|^2\,dt', \quad (2)$$

where $A(z,T)$ is the pulse envelope in the time domain; z represents the propagation distance; T is the delay in the time domain; β_2 and β_3 stand for the second-order and the third-order dispersion; α and γ are the linear loss and nonlinear coefficient in the fiber; g is the gain coefficient and can be expressed as[33,34]

$$g=\frac{g_0}{1+\frac{E_{\text{pulse}}}{E_{\text{sat}}}+\frac{(\omega-\omega_0)^2}{\Delta\omega_g^{\ 2}}}, \tag{3}$$

where g_0 represents the small signal gain, setting g_0=15.7 m^{-1}. E_{pulse} and E_{sat} represent the energy of the pulse and the gain saturation energy. Since the gain saturation energy is related to the pump power[33], its value can be tuned by changing the pump power. ω_0 and $\Delta\omega_g$ are the center angular frequency and the gain bandwidth. Raman response function $R(t)$ is given by[34]

$$R(t)=(1-f_R)\delta(t)+f_R h_R(t), \tag{4}$$

where f_R represents the fractional portion corresponding to the delay Raman and is set to 0.18, and $h_R(t)$ is the Raman response function of silica. For the SA based on the NPR technique, the transmittance can be expressed as[33]

$$T_{SA}=R_0+\mathrm{d}R\times\sin^2(\pi\times0.5\times P/P_A+\varphi), \tag{5}$$

where the phase delay φ is set to 0 for a simplicity. R_0 represents the minimum value of transmittance; dR is the modulation depth, corresponding to the variation range of SA transmittance. In addition, the transmittance curve is sinusoidal, with half the period equal to P_A. It is called positive saturation absorption that the transmittance of SA increases with instantaneous power. Otherwise, it is so-called reverse saturation absorption. The NLP states usually occur as a result of reverse saturation absorption[33].

In this paper, two kinds of filters are used in the simulation process: the Gaussian-shaped filter and the sinusoidal-shaped filter. The transmittance of the Gaussian-shaped filter can be written as[20]

$$T_f=\exp\left[-\frac{1}{2}\left(\frac{\omega-\omega_c}{2\omega_f}\right)^{2m}\right], \tag{6}$$

where ω_c is center angular frequency, and is defined by the filter bandwidth[20]

$$\omega_f=\frac{2\pi c}{(\lambda_c-\frac{\Delta\lambda}{2})(\lambda_c+\frac{\Delta\lambda}{2})}. \tag{7}$$

The sinusoidal-shaped filter can be expressed as[20]

$$T_f=\frac{1}{2}(T_{\max}-T_{\min})\cos\left[\frac{\pi(\omega-\omega_c)}{\omega_f}+\phi\right]+\frac{1}{2}(T_{\max}+T_{\min}), \tag{8}$$

where $T_{\max}$ and $T_{\min}$ represent the maximum and minimum transmittances of sinusoidal-shaped filter, respectively; and ϕ is the constant phase and set to 0 in the simulation. Since the sinusoidal-shaped filter with narrow bandwidth and large $T_{\min}$ is conducive to the generation of NLP[20], the filter bandwidth is set to 5 nm, while $T_{\max}$=0.99, and $T_{\min}$=0.9. In addition, the Gaussian-shaped filter bandwidth is set to 15 nm.

Fig.3 shows the intensity AC trace of NLP, where h_1 and h_2 represent the heights of the pedestal and peak, respectively. In order to analyze the influence of parameters on the intensity AC trace, the pedestal height ratio R_c is defined as follows:

$$R_c=\frac{h_2}{h_1+h_2}. \tag{9}$$

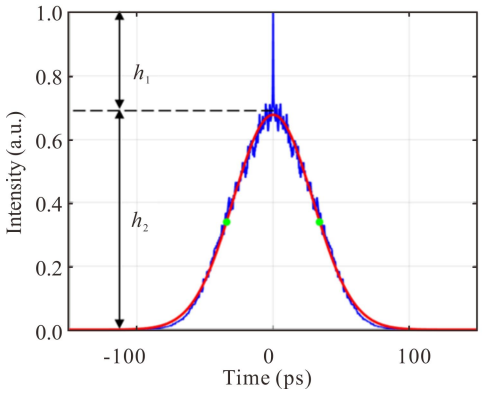

Fig.3 NLP intensity AC trace under Gaussian-shaped filter, when the net-cavity dispersion is 1.06 ps^2, E_{sat1}=0.8 nJ and E_{sat2}=0.4 nJ

The net-cavity dispersion of mode-locked laser can be tuned by adjusting the lengths of SMF and DCF. The gain saturation energies of EDF1 and EDF2 are represented by E_{sat1} and E_{sat2}, respectively. Fig.4 shows the effect of the gain saturation energy of EDF on the pedestal ratio of the NLP intensity AC, when the Gaussian-shaped filter is used and the net-cavity dispersion is fixed at 1.06 ps^2. As shown in Fig.4(a2)—(f2), it can be seen that under different E_{sat1} and E_{sat2}, the pedestal ratio R_c varies significantly from 0.82 to 0.57. When E_{sat1} and E_{sat2} are 0.1 nJ and 1 nJ, the DCF segment with normal dispersion plays a dominated role. And when E_{sat1} and E_{sat2} are 1.8 nJ and 0.2 nJ, the SMF segment with anomalous dispersion plays a dominated role. As a result, the output NLP exhibits a relatively high ratio R_c of 0.82 in Fig.4(a2). By contrast, when the anomalous SMF dominates the process of the pulse evolution with increasing E_{sat1} and decreasing E_{sat2}, the NLPs exhibit separated sub-pulses, accompanied by a decrease in pedestal ratio R_c.

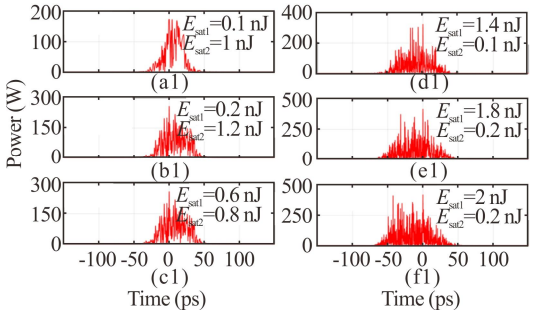

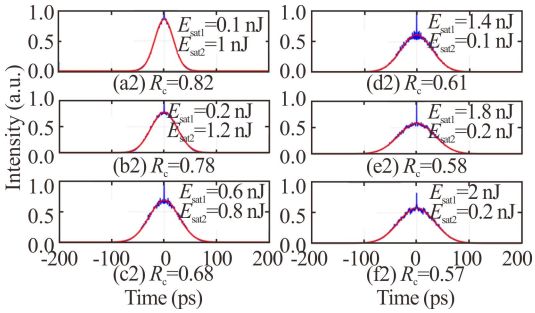

Fig.4 Output NLPs under different E_{sat1} and E_{sat2} when the net-cavity dispersion is 1.06 ps^2: (a1)—(f1) Pulse temporal envelopes; (a2)—(f2) Normalized intensity AC traces

When the net-cavity dispersion is still 1.06 ps^2, Fig.5 shows the R_c as a function of E_{sat1} or E_{sat2} in the cases with sinusoidal-shaped and Gaussian-shaped filters. When E_{sat1} remains unchanged, as shown in Fig.5(a) and (c), the curves of R_c exhibit flat shape with E_{sat2}. For example, in the case of sinusoidal-shaped filter with E_{sat1}=1 nJ, R_c remains nearly unchanged at around 0.6. Moreover, R_c decreases with E_{sat1} when E_{sat2} is fixed. However, R_c exhibits a large variation range. Especially when E_{sat2}=1 nJ, R_c has a largest variation range, which can be 0.56—0.88 and 0.61—0.82 in the cases with sinusoidal-shaped and Gaussian-shaped filters, respectively.

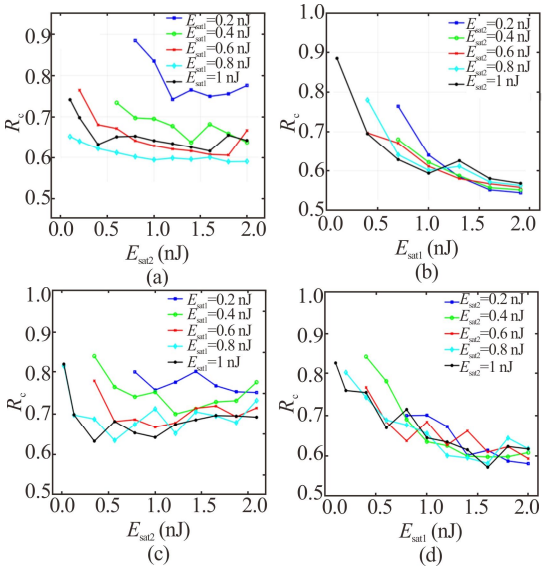

Fig.5 R_c curves of NLP intensity AC trace by using the (a, b) sinusoidal-shaped and (c, d) Gaussian-shaped filters ((a, c) R_c as a function of E_{sat2} with different E_{sat1}; (b, d) R_c as a function of E_{sat1} with different E_{sat2}; the net-cavity dispersion is 1.06 ps^2)

Fig.6 shows R_c as a function of both E_{sat1} and E_{sat2} in the cases with two kinds of filters, where the operation states of the fiber lasers include unstable state, single pulse and NLP. It can be seen that when both E_{sat1} and E_{sat2} are less than 0.5 nJ, the fiber lasers cannot obtain the mode locking and operate in the unstable state, as shown in Fig.6(b1) and (b2). When E_{sat2} increases beyond 0.5 nJ and reach up to near 1 nJ, the fiber lasers exhibit a wide tunable range of R_c by adjusting E_{sat1}, which can be 0.55—0.9 in the NLP sate and 1 in the single-pulse state.

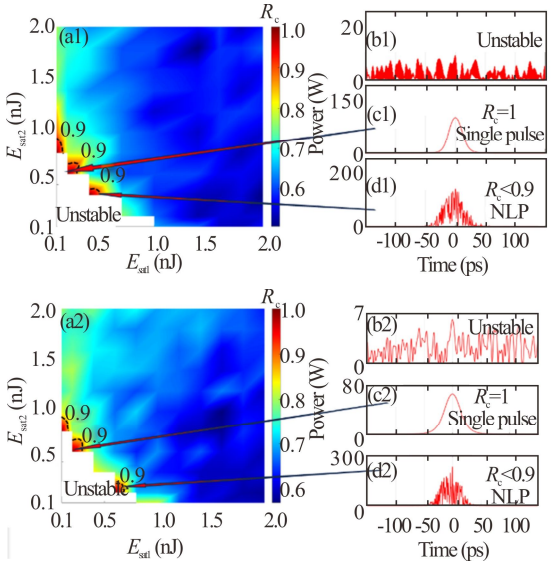

Fig.6 R_c of NLP intensity AC trace by using the (a1—d1) sinusoidal-shaped and (a2—d2) Gaussian-shaped filters ((a1, a2) R_c as a function of E_{sat1} and E_{sat2}; Temporal pulse envelopes in (b1, b2) are unstable; (c1, c2) Single pulse; (d1, d2) NLP states; The net-cavity dispersion is 1.06 ps^2)

Then, the influence of filter bandwidth $\Delta\lambda$ on the pedestal ratio of NLP intensity AC trace also needs to be analyzed, as shown in Fig.7. Again, in both cases with the sinusoidal-shaped and Gaussian-shaped filters, the fiber lasers exhibit more wide tunable range of R_c by adjusting E_{sat1} than those by varying E_{sat2}. Especially in the case of the Gaussian-shaped filter, when the bandwidth is in the range of 10—20 nm, R_c can be tuned from 0.55 to 0.9, as shown in Fig.7(c). In experiments, there are some ways to tune the filter bandwidth[35,36]. For example, the filter bandwidth can be tuned by controlling the distance between the reflection grating and collimator. The farther the distance, the smaller the bandwidth[36]. For sinusoidal-shaped filter, Lyot filter can be used, where the bandwidth of the filter can be changed by adjusting the splicing angle between the polarization-maintaining fiber and polarizer.

For the purpose of further analyzing the gain influence of two EDF segments on R_c, Fig.8 shows the variation range of R_c by tuning both E_{sat1} and E_{sat2} for the different filter bandwidths. It can be seen that the tunable ranges of R_c in NLP fiber lasers with sinusoidal-shaped filters are more sensitive to the filter bandwidth than those in NLP fiber lasers with Gaussian-shaped filters. Especially when the bandwidth of the sinusoidal-shaped filter is 5 nm, the tunable range of R_c can reach up to 0.51—0.88.

Finally, in order to observe the variation of R_c in the fiber lasers with different dispersion, Fig.9 shows the

variation range of R_c by adjusting both E_{sat1} and E_{sat2}, when the net-cavity dispersion is tuned from −1.443 ps^2 to 1.8 ps^2. The net-cavity dispersion of the fiber laser can be changed by tailoring the lengths of SMF and DCF. It is noteworthy that the NLP fiber lasers with the normal net-cavity dispersion can exhibit a wider tunable range of R_c than those with the anomalous net-cavity dispersion. Especially when the net-cavity dispersion is 1.06 ps^2, R_c variation ranges can reach up to 0.51—0.89 and 0.58—0.88 for the cases with the sinusoidal-shaped and Gaussian-shaped filters.

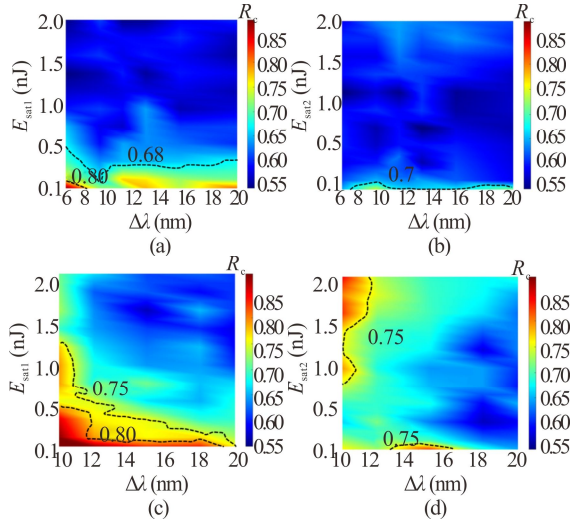

Fig.7 R_c of NLP intensity AC trace by using (a, b) sinusoidal-shaped and (c, d) Gaussian-shaped filters ((a, c) R_c as a function of E_{sat1} and $\Delta\lambda$ when E_{sat2}=1 nJ; (b, d) R_c as a function of E_{sat2} and $\Delta\lambda$ when E_{sat1}=1 nJ; The net-cavity dispersion is 1.06 ps^2)

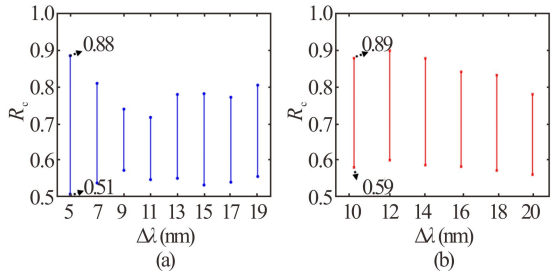

Fig.8 Variation range of R_c by tuning E_{sat1} and E_{sat2} with different filter bandwidths for (a) sinusoidal-shaped and (b) Gaussian-shaped filters

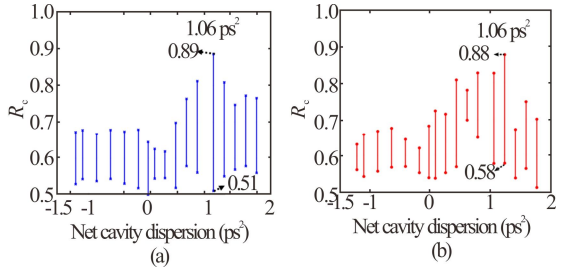

Fig.9 Tunable range of R_c by using (a) the sinusoidal-shaped filter with $\Delta\lambda$=5 nm, and (b) the Gaussian-shaped filter with $\Delta\lambda$=15 nm, where the net-cavity dispersion is from −1.443 ps^2 to 1.8 ps^2

In conclusion, a novel method of tuning the pedestal ratio R_c of the intensity AC trace for the NLPs is presented based on the EDF mode-locked lasers, featured by two pieces of gain fibers, which are followed by normal and anomalous dispersion fibers. The influences of gain saturation energies of two EDF segments, i.e., E_{sat1} and E_{sat2}, filter bandwidth, and net-cavity dispersion on the ratio R_c are investigated by numerical simulations. The results show that the NLP fiber lasers with the sinusoidal-shaped filter and normal net-cavity dispersion can obtain a wider range of R_c than those with the Gaussian-shaped filter and anomalous net-cavity dispersion. Therefore, the optimal conditions for obtaining a broad variable range of R_c are the net-cavity dispersion of 1.06 ps^2, and the sinusoidal-shaped filter with a bandwidth of 5 nm. Under the circumstances, the pedestal ratio R_c can be tuned from 0.51 to 0.89 by adjusting parameters E_{sat1} and E_{sat2} in the range of 0.1—2 nJ.

Ethics declarations

Conflicts of interest

The authors declare no conflict of interest.

References

[1] SERGEY S, SERGEY K, SERGEY K, et al. Three key regimes of single pulse generation per round trip of all-normal-dispersion fiber lasers mode-locked with nonlinear polarization rotation[J]. Optics express, 2012, 20(24): 27447-27453.

[2] NELSON L E, JONES D J, TAMURA K, et al. Ultrashort-pulse fiber ring lasers[J]. Applied physics, 1997, B65(2): 277-294.

[3] HAN X X. Conventional soliton or stretched pulse delivered by nanotube-mode-locked fiber laser[J]. Applied optics, 2018, 57(4): 807-811.

[4] CHONG A, WRIGHT L G, WISE F W. Ultrafast fiber lasers based on self-similar pulse evolution: a review of current progress[J]. Reports on progress in physics, 2015, 78(11): 113901.

[5] GRELU P, AKHMEDIEV N. Dissipative solitons for mode-locked lasers[J]. Nature photonics, 2012, 6(2): 84-92.

[6] CHANG W, ANKIEWICZ A, SOTO-CRESPO J M, et al. Dissipative soliton resonances[J]. Physical review E, 2008, 78(2): 023830.

[7] HOROWITZ M, BARAD Y, SILBERBERG Y. Noise-like pulses with a broadband spectrum generated from an erbium-doped fiber laser[J]. Optics letters, 1997, 22(11): 799-801.

[8] LI X, ZHANG S, LIU J, et al. Using reverse saturable absorption to boost broadband noise-like pulses[J]. Journal of lightwave technology, 2020, 38(14): 3769-3774.

[9] MENG F, LAPRE C, BILLET C, et al. Intracavity incoherent supercontinuum dynamics and rogue waves in

a broadband dissipative soliton laser[J]. Nature communication, 2021, 12: 5567.

[10] LI C, KONG C, WONG K K Y. High energy noise-like pulse generation from a mode-locked thulium-doped fiber laser at 1.7 μm[J]. IEEE photonics journal, 2019, 99: 1.

[11] BOUCON A, BARVIAU B, FATOME J, et al. Noise-like pulses generated at high harmonics in a partially-mode-locked km-long Raman fiber laser[J]. Applied physics, 2012, 106(2): 283-287.

[12] LI J, WANG C, WANG P. Tunable noise-like pulse and Q-switched erbium-doped fiber laser[J]. Optics express, 2022, 30(4): 4768-4781.

[13] MASHIKO Y, FUJITA E, TOKURAKAWA M. Tunable noise-like pulse generation in mode-locked Tm fiber laser with a SESAM[J]. Optics express, 2016, 24(23): 26515.

[14] LI X, ZHANG S, YANG Z. Noise-like pulse fiber lasers[C]//2022 20th International Conference on Optical Communications and Networks (ICOCN), August 12-15, 2022, Shenzhen, China. New York: IEEE, 2022: 1-3.

[15] KEREN S, HOROWITZ M. Interrogation of fiber gratings using spectral interferometry of a low-coherence light source[C]//Conference on Lasers & Electro-Optics, May 7-12, 2000, San Francisco, CA, USA. New York: IEEE, 2020.

[16] MARSCHALL S, KLEIN T, WIESER W, et al. Fourier domain mode-locked swept source at 1050 nm based on a tapered amplifier[J]. Optics express, 2010, 18(15): 15820.

[17] KEREN S, BRAND E, LEVI Y, et al. Data storage in optical fibers and reconstruction by use of low-coherence spectral interferometry[J]. Optics letters, 2022, 27(2): 125-127.

[18] SERGEY K, SERGEY K, SERGEY S, et al. Generation of double-scale femto/picosecond optical lumps in mode-locked fiber lasers[J]. Optics express, 2009, 17(23): 20707.

[19] ZHAO Q, PAN W W, ZENG X L, et al. Partially coherent noise-like pulse generation in amplified spontaneous Raman emission[J]. Applied optics, 2018, 57(9): 2282-2286.

[20] XU R Q, XU F J, SONG Y R, et al. Impact of spectral filtering on pulse breaking-up and noise-like pulse generation in all-normal dispersion fiber lasers[J]. Optics express, 2020, 28(15): 21348-21358.

[21] LI X L, ZHANG S M, LIU J M, et al. Efficient method to improve the distribution probability of dissipative soliton and noise-like pulse in all-normal-dispersion fiber lasers[J]. Optics express, 2022, 30(4): 6161-6175.

[22] LIU S, YAN F, LI Y, et al. Noise-like pulse generation from a thulium-doped fiber laser using nonlinear polarization rotation with different net anomalous dispersion[J]. Photonics research, 2016, 4(6): 318-321.

[23] TANG D Y, ZHAO L M, ZHAO B. Soliton collapse and bunched noise-like pulse generation in a passively mode-locked fiber ring laser[J]. Optics express, 2005, 13(7): 2289-2294.

[24] LEI D, YANG H, DONG H, et al. Effect of birefringence on the bandwidth of noise-like pulse in an erbium-doped fiber laser[J]. Journal of modern optics, 2009, 56(4): 572-576.

[25] DONG T H, LIN J Q, ZHOU Y, et al. Noise-like square pulses in a linear-cavity NPR mode-locked Yb-doped fiber laser[J]. Optics and laser technology, 2021, 136(1): 106740.

[26] LUO A P, LUO Z C, LIU H, et al. Noise-like pulse trapping in a figure-eight fiber laser[J]. Optics express, 2015, 23: 10421.

[27] XU R Q, TIAN J R, SONG Y R. Noise-like pulses with a 14.5 fs spike generated in an Yb-doped fiber nonlinear amplifier[J]. Optics letters, 2018, 43(8): 1910.

[28] LAUTERIO-CRUZ J P, HERNANDEZ-GARCIA J C, POTTIEZ O, et al. High energy noise-like pulsing in a double-clad Er/Yb figure-of-eight fiber laser[J]. Optics express, 2016, 24(13): 13778-13787.

[29] TANG Y X, LIU Z W, FU W, et al. Self-similar pulse evolution in a fiber laser with a comb-like dispersion-decreasing fiber[J]. Optics letters, 2016, 41(10): 2290-2293.

[30] YOFC dispersion compensating fiber (DCF)[EB/OL]. (2023-01-25) [2023-05-26]. http://en.yofc.com/view/2370.html.

[31] LIU Z, ZHANG S, WISE F W. Rogue waves in a normal-dispersion fiber laser[J]. Optics letters, 2015, 4: 1366-1369.

[32] GENIER E, BOWEN P, SYLVESTRE T, et al. Amplitude noise and coherence degradation of femtosecond supercontinuum generation in all-normal-dispersion fibers[J]. Journal of the optical society of America B, 2019, 36(2): A161.

[33] CHENG Z C, LI H H, WANG P. Simulation of generation of dissipative soliton, dissipative soliton resonance and noise-like pulse in Yb-doped mode-locked fiber lasers[J]. Optics express, 2015, 23(5): 5972-5981.

[34] DUDLEY J M, GENTY G, STÉPHANE C. Supercontinuum generation in photonic crystal fiber[J]. Review of modern physics, 2006, 78: 1135.

[35] ZAYTSEV A K, LIN C H, YOU Y J, et al. A controllable noise-like operation regime in a Yb-doped dispersion-mapped fiber ring laser[J]. Laser physics letters, 2013, 10(4): 045104.

[36] ZHANG Z C, WANG S, PU Y J, et al. Improving the formation probability and stability of noise-like pulse by weakening the spectrum filtering effect[J]. Optics express, 2012, 30(18): 31998-32009.